



Thermally-Induced Wedging–Ratcheting Failure Mechanism in Rock Slopes

Dagan Bakun-Mazor¹ · Yuval Keissar² · Aviran Feldheim² · Christine Detournay³ · Yossef H. Hatzor²

Received: 6 August 2019 / Accepted: 18 February 2020
© Springer-Verlag GmbH Austria, part of Springer Nature 2020

Abstract

A thermally induced wedging–ratcheting mechanism for slope stability is investigated using a large-scale physical model and using a three-dimensional version of the numerical Distinct Element Method (3DEC). The studied mechanism consists of a discrete block that is separated from the rock mass by a tension crack filled with a wedge block or rock fragments. Irreversible block sliding is assumed to develop down a gently dipping sliding plane in response to climatic thermal fluctuations and consequent contraction and expansion of the sliding and wedge block materials. A concrete block assembly representing the rock mass is placed in a specially designed climate controlled room. An integrated measurement system tracks the block displacement and temperature evolution over time. Results of the numerical 3DEC model and an existing analytical solution are compared with the experimental results and the sensitivity of the numerical and analytical solutions to the input thermo-mechanical parameters is explored. To test the applicability of our physical and numerical models to the field scale, we compare our numerical simulations with monitored displacements of a slender block that was mapped in the East slope of Mount Masada, as up until recently the governing mechanism for this block displacement has been assumed to be seismically driven. By application of our numerical approach to the physical dimensions of the block in the field we find that, in fact, thermal loading alone can explain the mapped accumulated displacement that has surpassed by now 200 mm. We believe this new, thermally-induced, failure mechanism may play a significant role in slope stability problems due to the cumulative and repetitive nature of the displacement, particularly in rock slopes in fractured rock masses that are exposed to high temperature oscillations.

Keywords Rock slope stability · Coupled thermo-mechanical response · Discrete element method · 3DEC · Wedging mechanism · Climate controlled room

1 Introduction

Cumulative block displacement in rock slopes may occur in response to various environmental factors, including seismic vibrations, water pressures in discontinuities, freezing and thawing of water in discontinuities, and thermal fluctuations in the rock mass. The influence of the latter mechanism on the stability of rock slopes has been known for some time,

but is still not well understood. Several monitoring surveys have detected slow, creep-like, slope displacements due to cyclic temperature changes in the field (e.g. Hatzor et al. 2002; Hatzor 2003; Watson et al. 2004; Gunzburger et al. 2005; Greif et al. 2006; Vicko et al. 2009; Gischig et al. 2011a; Gischig et al. 2011b; Mufundirwa et al. 2011; Vargas et al. 2013; Taboada et al. 2017).

Although temperature changes are cyclical, they can cause cumulative deformations in systems where there is a preferred directionality of the sliding surface. This was shown and discussed by Gunzburger et al. (2005), and referred to as “crawling motion”. Moreover, asymmetry in the blocky system leads to the development of preferred directional stresses that are able to induce permanent displacement of rock blocks.

Recently, a thermally-induced “wedging–ratcheting mechanism” has been proposed as a new failure mode in

✉ Dagan Bakun-Mazor
daganba@sce.ac.il

¹ Department of Civil Engineering, Shamoon College of Engineering, Beer-Sheva, Israel

² Department of Geological and Environmental Sciences, Ben-Gurion University of the Negev, Beer-Sheva, Israel

³ Itasca Consulting Group Inc, Minneapolis, MN, USA

rock slopes that has to be considered in the relevant geological and climatic settings (Bakun-Mazor et al. 2013; Pasten 2013). A conceptual model of thermally-induced block sliding is schematically illustrated in Fig. 1a. In this wedging mechanism, it is assumed that the block assemblage contracts when the air cools. The tension crack thus opens, and consequently the wedge block slides into the newly formed opening in the tension crack (Fig. 1b). When the temperature is increased, the sliding block is expected to expand but the wedge block will now be locked in place, prompting compressive stress generation in the block system, and if frictional resistance is insufficient, the sliding block may slide down the dip of the sliding plane (Fig. 1c). Photos of some typical geometries of rock blocks in the field that may be susceptible to the proposed failure mechanism, are shown in Fig. 2.

1.1 Theoretical Considerations

Following the analytical expression suggested by Pasten (2013), three displacement components are involved in the process: thermal expansion (δ_T), elastic compression of the rock material (δ_σ), and elastic shear response along the sliding interface (δ_j). The unconstrained cyclic thermal expansion (δ_T) on both sides of the tension crack, as well as the wedge block inside the tension crack, may be expressed by:

$$\delta_T = \alpha \cdot \Delta T_p \cdot d(t_{\text{exp}}) \quad (1)$$

where α is the thermal expansion coefficient of the intact rock, ΔT_p is the cyclic temperature change, and $d(t_{\text{exp}})$ is the length of material subjected to expansion. Note that $d(t_{\text{exp}})$ is a function of the exposure period of the thermal fluctuation, t_{exp} . Assuming t_{exp} is large enough to homogeneously affect the entire blocky system, $d(t_{\text{exp}})$ may be assumed to cover both the wedge and the sliding block, and equals to $L_w + L_b$ (see Fig. 3). If t_{exp} is not large enough, a parameter that takes into account the depth of penetration of the thermal front during a single cycle, referred to as skin depth, S_d , should be introduced (Pasten 2013; Pasten et al. 2015b).

During a thermal expansion period, uniform compressive stresses develop in the domain, leading to an elastic force within the block. Following Pasten (2013) and considering the block configuration in Fig. 3, the maximum force parallel to the sliding surface required for limit equilibrium (F_{max}) is (for complete derivation see Appendix 1):

$$F_{\text{max}} = \gamma (\cos \eta_1 \tan \phi - \sin \eta_1) \left[L_b H_b + \frac{L_{w1} + L_{w2}}{2} H_w \right] \quad (2)$$

Here γ is the unit weight of the rock ($\gamma = \rho g$), ϕ is the friction angle of the sliding plane, L_b and L_w are the lengths of the sliding block and the wedge, respectively, H_b and H_w are the heights of the sliding block and wedge, respectively, η_1 is the inclination of the sliding plane, η_2 is the inclination of the wedge. The elastic displacement δ_σ that is developed in the wedge and the block due to F_{max} is:

$$\delta_\sigma = \frac{F_{\text{max}}}{H_b \cdot E} \left(L_w + \frac{L_b}{2} \right) \quad (3)$$

where E is the modulus of elasticity of the rock material. Finally, assuming that the toe of the block (the lower right corner of the sliding block in Fig. 3) is static during the expansion period, the elastic displacement of the interface parallel to the sliding direction δ_j due to F_{max} is:

$$\delta_j = \frac{F_{\text{max}}}{k_j L_b} \quad (4)$$

where k_j is the shear stiffness of the sliding interface.

It is important to note that the elastic components derived in both Eqs. 3 and 4 are the result of the maximum resistance force (F_{max}), namely the reaction that can accumulate parallel to the sliding plane, before the joint displacement overcomes the elastic threshold [for more details see Pasten et al. (2015b)]. During cyclic thermal heating, a permanent displacement is expected when:

$$\delta_T > \delta_\sigma + \delta_j \quad (5)$$

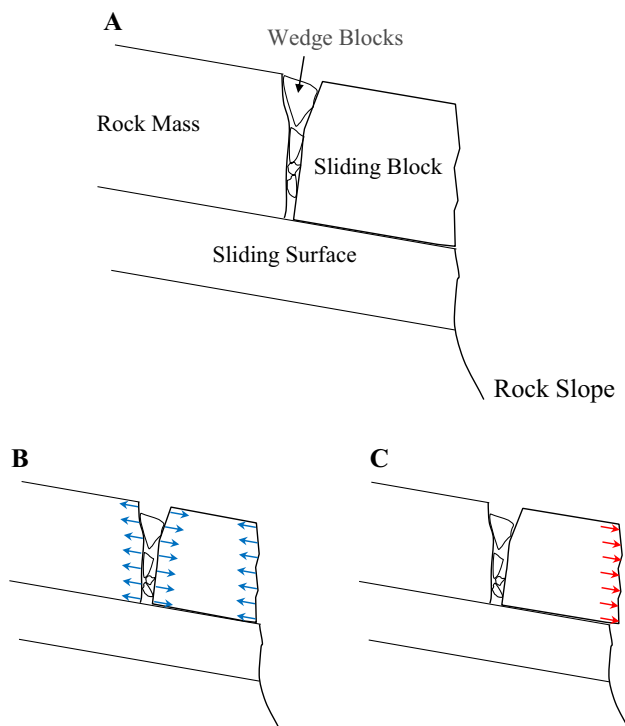


Fig. 1 The thermally-induced wedging–ratcheting mechanism in discontinuous rock slopes, **a** structural components, **b** cooling episode, and **c** heating episode (after Bakun-Mazor et al. 2013)

Fig. 2 Photos of blocks from the field that illustrate the wedging mechanism, **a** Masada Mountain, Israel, **b** Ramon Crater, Israel, **c** Arugot Valley, Israel, and **d** Yellow Mountain, China. The scale of each bar in the inset represents 1 m

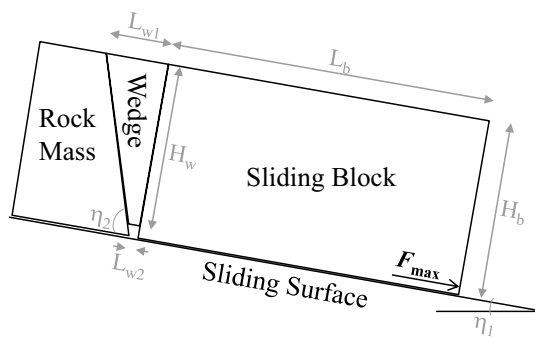
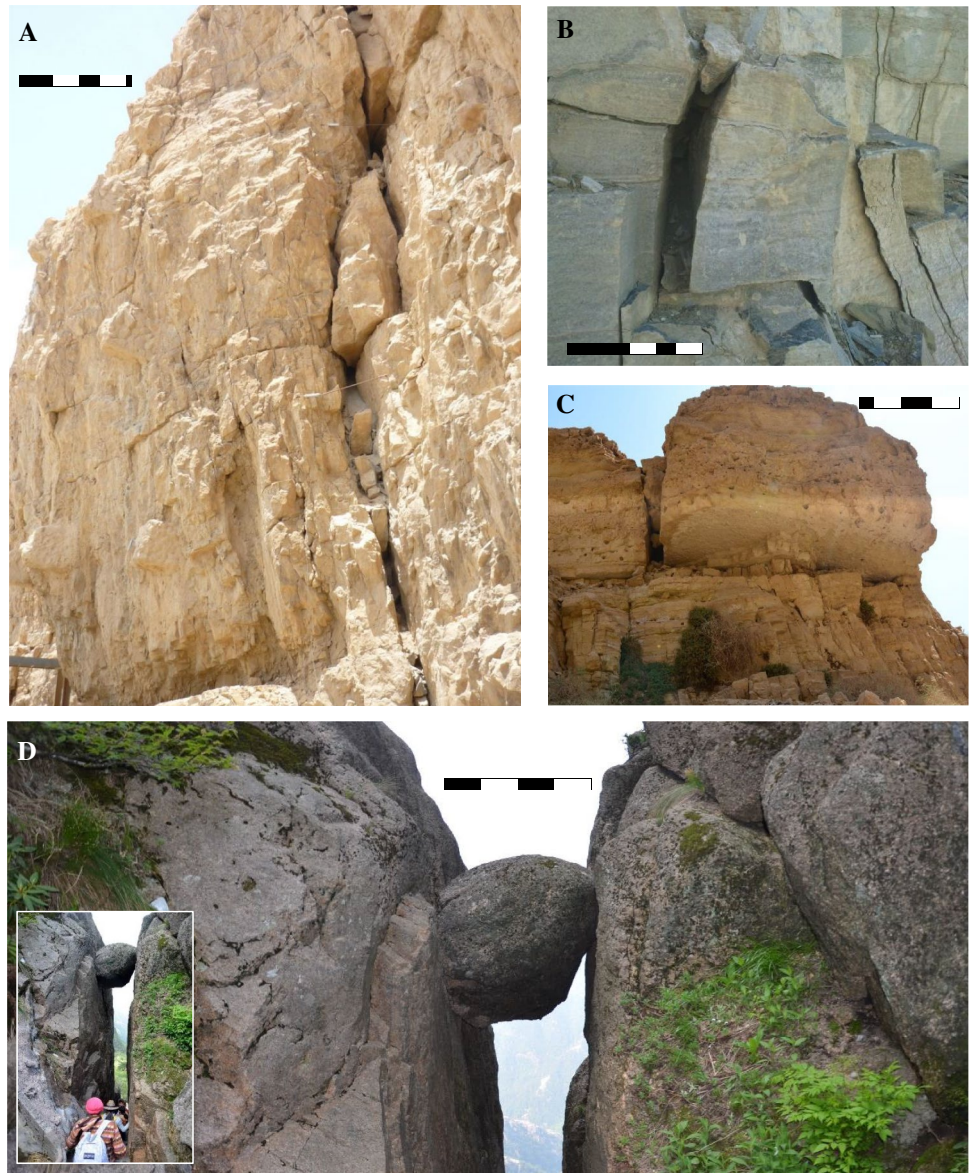


Fig. 3 Description of the elements in the analytical model

1.2 Previous Experimental Work

Pasten et al. (2015b) investigated the thermally-induced ratcheting mechanism on a 350×225 mm physical model made of acrylic blocks that react against an aluminum base and a back wall, using a temperature-controlled chamber. They showed that the thermal cycles do prompt gradual downward displacement of the wedge. Their analytical expression reviewed above was compared to the experimental results in terms of the critical thermal fluctuation required to initiate block displacement, and a good agreement at varied geometries and periods of the cyclic thermal loading was reported. They showed that the simplified analytical solution is in agreement with numerical results, as long as the exposure time is large enough. They concluded that the thermo-mechanical coupling can lead to permanent displacements

when a rock mass is subjected to a biased static-force condition, where there is a preferred directionality of the sliding surface, and that the permanent displacements are accentuated by the intensity of the biased force, the amplitude of the thermal cycle, the exposure time, the thermal expansion coefficient of the rock, and the joint brittleness (i.e. the threshold deformation for elastic-to-plastic transition). Subsequently, Pasten et al. (2015a) showed experimentally and numerically that the displacement accumulation is proportional to the combination of the amplitude and period of the temperature cycle (ΔT_p and t_{exp} in Eq. 1). In addition, the conditions for failure modes of toppling and sliding were identified, both analytically and numerically.

Greif et al. (2014) tested the thermally induced wedging mechanism on nine sets of 50 mm sandstone specimens using thermal dilatometer. They confirmed that the suggested mechanism leads to cumulative deformation, and that the measured threshold temperature change at which block deformation occurs, is in agreement with the analytical solution proposed by Pasten (2013).

Yet, the experimental setups, both of Pasten et al. (2015a) and Greif et al. (2014), were of relatively small dimensions (length scales in the order of 10^{-3} to 10^{-1} m), where a single displacement sensor measured the cumulative response of the entire system. It is nevertheless very important to determine if this failure mechanism can develop in block systems at the scale of removable rock blocks in the field, to determine the role the wedge plays in this process, and to address the significance of the mechanism in real slope stability analyses.

2 Large-Scale Physical Model Inside a Climate Controlled Room

2.1 Setup of the Physical Model

The physical model consists of an assemblage of concrete blocks. A lower block serves as a sliding surface, and above it three blocks are positioned: a sliding block, a fixed block representing the rock mass, and a wedge in the space between that represents the tension crack in the field (Fig. 4). The components of the concrete mixture are: Portland cement 36%, fine quartz sand aggregates 41%, coarse limestone aggregates 7%, water 17%. The block assembly is situated on an inclined steel table that tilts the block system at 15 degrees above the horizon. A plastic sheet (HDPE) smeared with grease separates the table from the block system to serve as a substrate that isolates the thermal reaction of the steel table.

The block system on the tilted table is placed inside the Climate Controlled Room (CCR) located in the Department of Environmental Hydrology and Microbiology, Zuckerberg

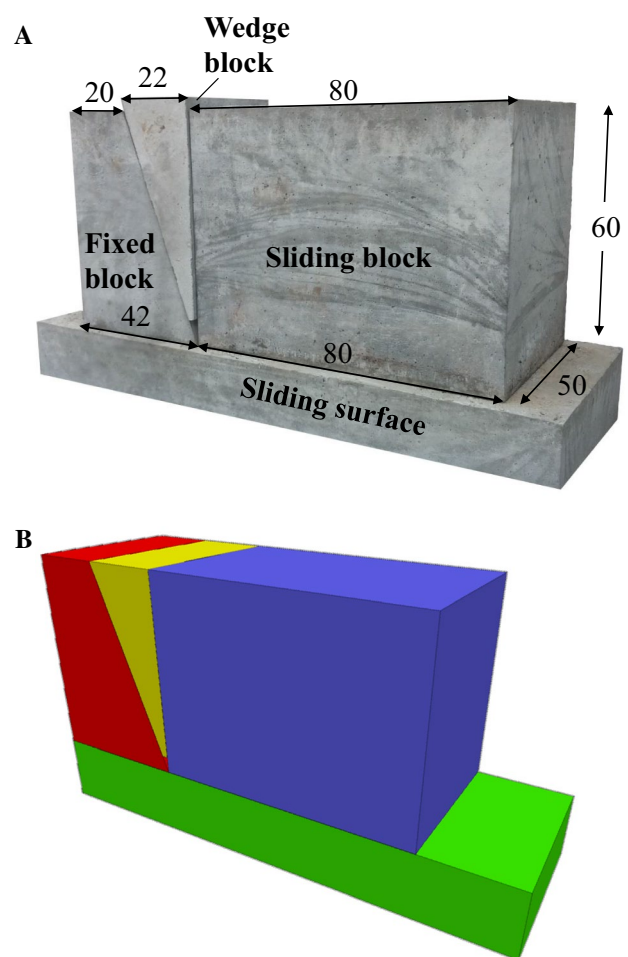
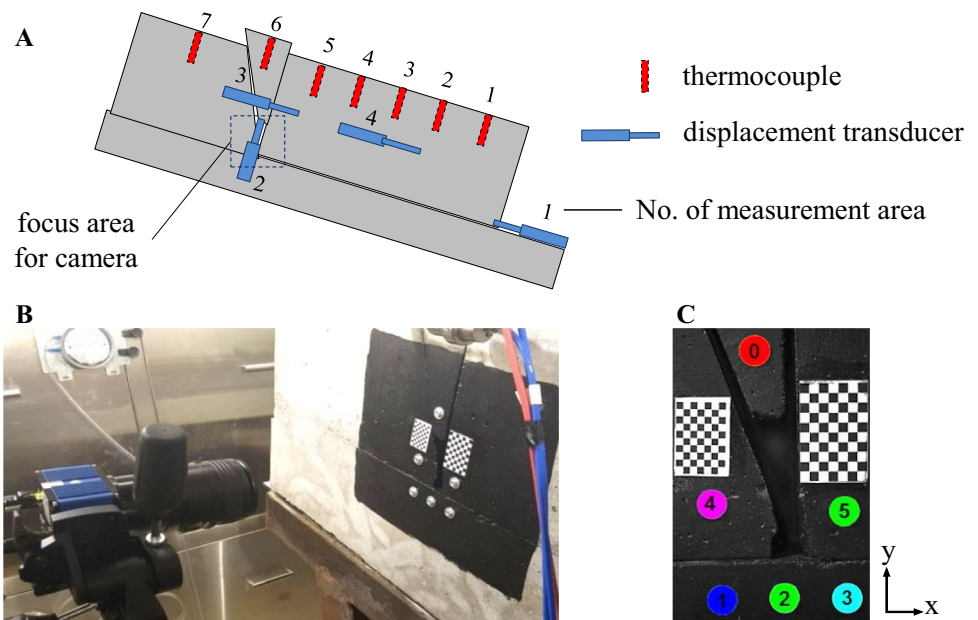


Fig. 4 a The block system that makes up the physical model, before placing on the inclined table and inserting to the CCR. Blocks dimensions are in cm. b Snapshot from the 3DEC numerical model

Institute for Water Research, at Ben-Gurion University. Both cooling and heating are provided in the room by radiation from cold or hot air, flowing between two walls in a closed system at the upper part of the room, applied by means of a large air-conditioning facility. No wind is allowed to flow in the laboratory while the temperature is being controlled. This capability enables the impact of temperature variation to be separated from that of other atmospheric conditions, especially wind.

Two sets of displacement transducers are installed on the blocky system: Vibrating Wire (VW) set model EDJ-40 V (ENCARDIO RITE 2015) and Potentiometer (PM) set model DS-810 (SIM STRUMENTI 2009). The displacement transducers function as joint meters while the ends of each transducer are fixed to one of the blocks, and the relative displacement between two blocks is measured. Four transducers (both VM and PM) are installed across four areas in the tested assembly. The measurement areas for the displacement transducers are shown in Fig. 5a. In

Fig. 5 Layout of the measurement system that detect blocks displacement and temperature profile inside the blocks in the physical model when placed inside the CCR



measurement area #1 the relative displacement between the sliding block and the lower surface is monitored. In measurement area #2 the relative displacement between the wedge and the lower surface is measured. In measurement area #3 the relative displacement between the fixed block and the sliding block is measured. Transducer 4 is installed on the intact block, for control.

A high-resolution (6576×4384 pixels) visual range camera tracks the focus area (15.95 cm in height and 10.30 cm in width) between the wedge, the fixed block, and the sliding block (see Fig. 5b). Within the focus area six screws are drilled and attached to the blocks in order to serve as marker points for image processing. Point 0 is located on the wedge, points 1–3 on the lower surface, point 4 on the fixed block, and point 5 on the sliding block (Fig. 5c). During the image processing the coordinates of the centers of the screws are found, and the relative distances between those centers are calculated, with accuracy of a single pixel at ± 0.024 mm. Photos are taken every 15 min.

A series of T-type thermocouples are implanted into the concrete blocks in order to measure the temperature variation within the blocks during the experiment inside the CCR. The thermocouples, with accuracy of ± 0.5 °C and temperature range of -18 °C to $+100$ °C, are installed before casting, every 30 cm along the central inner axis of the block system (Fig. 5a).

2.2 Material Properties

The properties of the concrete material from which the model blocks were prepared are fully determined in lab experiments in order to validate the analytical solution with results obtained from the physical model experiment. The experimental processes and the obtained results are given in detail in Feldheim (2017). The experimentally obtained material properties of the concrete are summarized in Table 1. These properties are used as input parameters in the analytical solution described above (Eqs. 1–5). The results of the analytical solution are provided in the discussion section

Table 1 Thermomechanical properties of the concrete used for the experiments

| | Parameter | Symbol | Units | Value |
|---------------------|----------------------------------|----------|--------------------------------|--------|
| Material properties | Elastic modulus | E | GPa | 24.486 |
| | Poisson's ratio | ν | – | 0.2513 |
| | Bulk density | ρ | kg/m ³ | 2140 |
| Joint properties | Friction angle | ϕ | ° | 21.28 |
| | Normal stiffness | K_n | GPa/m | 5 |
| | Shear stiffness | K_s | GPa/m | 0.5 |
| Thermal properties | Thermal expansion coefficient | α | $10^{-6}/^{\circ}\text{C}$ | 3.22 |
| | Thermal diffusivity | D_T | $10^{-7}\text{m}^2/\text{sec}$ | 5.44 |
| | Specific heat capacity (assumed) | C_p | J/kg/K | 850 |

where a comparison between the analytical solution and the measured displacement in the physical model is made.

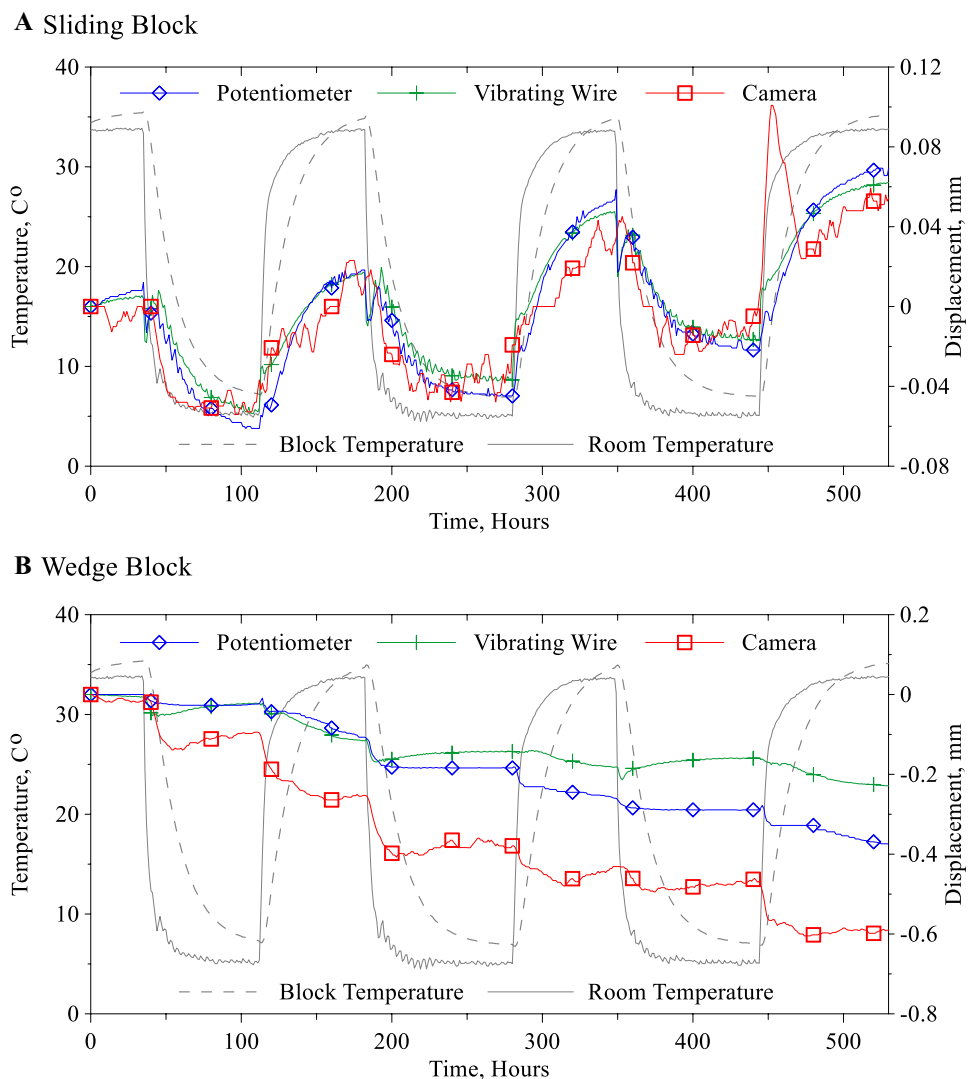
2.3 Results of Physical Model Experiments

The block assembly described in Sect. 2.1 is inserted into the CCR for the duration of the experiment period. First, the exposure time required for the block center to reach the target temperature in the room is studied. The room temperature is elevated to 35 °C and held at that temperature while the thermocouples at the center of the block reach that temperature. Then, the room temperature is cooled to 5 °C and the time required for the center of the block to cool to that temperature is monitored. This procedure is repeated alternately. While the room temperature is changed during approximately 3 h, the center of the block reaches the target temperature after approximately 72 h. By waiting for the center of the block to reach the target temperature, it is assumed that t_{exp} is large enough to distribute homogeneously

throughout the block system. It is important to emphasize that the boundary conditions applied during the experiments simulate seasonal, rather than daily, temperature changes, as we assume that t_{exp} of daily changes is too short for the temperature profile to penetrate sufficiently deep into the block to affect the studied mechanism. Therefore, sun radiation during daytime, thermal emissions from the rock during nighttime, or wind effects on surface temperature, are not considered here.

The displacement response, obtained by three different measurement methods, is shown in Fig. 6. The relative displacement between the fixed block and the sliding block (measurement area #3 in Fig. 5) is plotted in Fig. 6a; the relative displacement between the wedge and the lower surface (measurement area #2 in Fig. 5) is plotted in Fig. 6b. As can be seen in Fig. 6a, there is great consistency in the results obtained from the three different measurement methods. The cumulative displacement of the sliding block along three thermal cycles, as obtained from all displacement methods,

Fig. 6 Physical model results. Displacement obtained by three different measurement methods (colored lines) is shown on the right y-axis, room and block temperature (gray lines) are shown on the left y-axis, for **a** sliding block, and **b** wedge block (color figure online)



is between 0.053 to 0.069 mm (namely displacement rate of 0.018 to 0.023 mm per thermal cycle). During the three thermal cycles, the wedge block incised down into the tension crack by 0.23 to 0.59 mm (Fig. 6b). It should be noted that room temperature is measured at the lower part of the room, under the block setup, which explains the gap of two degrees between room and block temperature, as arrived in Fig. 6.

2.4 Result comparison with the analytical solution

We now compare the measured displacement rate in the physical model with results obtained from the analytical solution. Displacement rates obtained from the analytical solution (Eqs. 1–5) for a range of linear thermal expansion coefficients and shear stiffnesses are plotted in Fig. 7, with all other input material properties as listed in Table 1.

The rate calculated by the analytical model with the governing material properties as measured by us for the intact material and interface, i.e. linear thermal expansion coefficient α of $3.22 \times 10^{-6} \text{ } 1^\circ\text{C}$ and shear stiffness k_j of 500 kPa/mm, is shown in Fig. 7 as an open white circle (0.082 mm/cycle). For comparison, the displacement rate obtained when simulating the model with 3DEC (see next section) is plotted in Fig. 7 as an open white triangle (0.096 mm/cycle), when all other input parameters are as listed in Table 1. Finally, the displacement rate of 0.02 mm/cycle as measured in the physical model (see previous section) is plotted as a white dashed line in Fig. 7.

It is interesting to note that both the analytical and numerical approaches converge to the same displacement rates, between 0.082 and 0.096 mm/cycle, within 1% difference. This suggests that the rather simple analytical solution can be useful for rapid assessment of anticipated displacement rates of blocks in rock slopes that are prone to the analyzed failure mechanism. It is important to emphasize however that during the experiment and in the numerical simulations (see next section), the target temperature imposed on the system

remains constant for long enough time until the center of the sliding block equilibrates under the same target temperature. For shorter exposure periods Pasten et al. (2015b) employed the “skin depth” parameter that is not studied here experimentally.

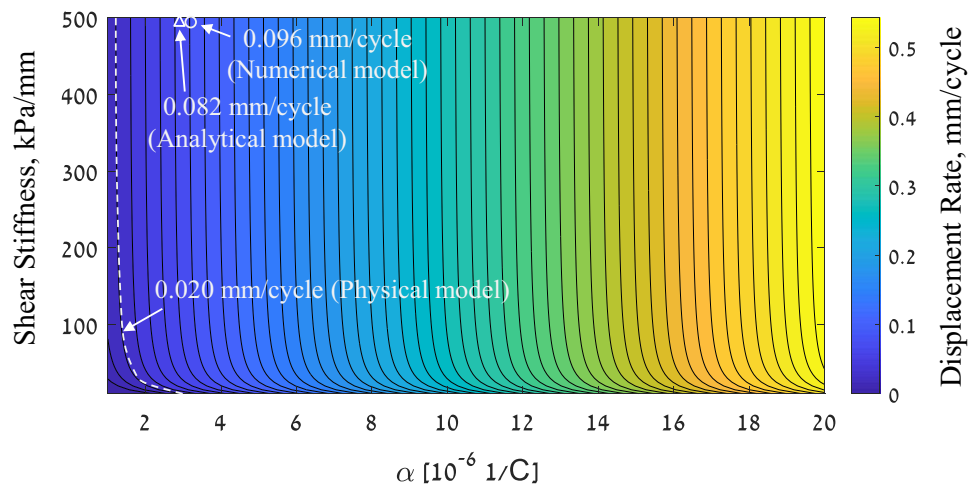
Both the analytical solution and the numerical simulations yield displacement rates four times higher than the displacement rate measured in the physical model. This could be explained by the high sensitivity of both solutions to the input value of the linear thermal expansion coefficient, α as the sensitivity of the solutions to the input value of the joint shear stiffness appears to be much lower (see Figs. 7 and 9 below).

A possible reason for the discrepancy between the experiment and the theoretical models may be due to the material properties determined in lab. The theoretical models used for input material properties that were obtained from small lab samples, with dimensions in order of 10^{-2} to 10^{-1} m, while the physical model is composed by blocks two orders of magnitudes larger. The possibility of a scale effect in the input parameters can explain the difference in the results obtained in the different approaches studied here.

3 Numerical Study with 3DEC

The proposed wedging–ratcheting mechanism is studied numerically using the Distinct Element Method (DEM) code 3DEC (Itasca Consulting Group 2013) developed by Cundall and colleagues (Cundall 1988; Hart et al. 1988; Cundall and Hart 1992). The theoretical foundation of this method is the formulation and solution of equations of motion of deformable blocks by an explicit (using Finite Volume Method) time marching scheme (Jing 2003). The code can simulate the response of discontinuous media to static, dynamic or thermal loading and provide the corresponding deformation.

Fig. 7 Calculated displacement rate based on the analytical model, for different values of linear thermal expansion coefficient, α , and shear stiffness, k_j . The rest of the parameters are listed in Table 1. The geometry is according to the physical model. Dashed line represents displacement rate of 0.02 mm/cycle as measured in the physical model tests



The physical model geometry is reproduced in 3DEC (Fig. 4b). Block discretization is achieved using a uniform mesh with an average edge length of 5 cm. Thermo-mechanical properties (Table 1) are assigned to the concrete mass and the interfaces. Boundary conditions, in particular the temperature time-histories, are applied on all exposed faces of the three-dimensional model. The model is fixed in the normal direction behind the rock mass, and in all directions at the bottom of the sliding surface.

Forward 3DEC simulations begin after initial equilibrium is obtained. Before any thermal loading is applied, and under gravity only, the model is adjusted to block cutting, mesh generation, and to the applied boundary conditions. An elastic stress field is applied by running the model until force equilibrium is reached. During that process, blocks settle, and some displacement takes place across the joints. Displacement histories of the sliding block and the wedge are recorded for grid points at the exact same locations where the displacement meters in the physical model

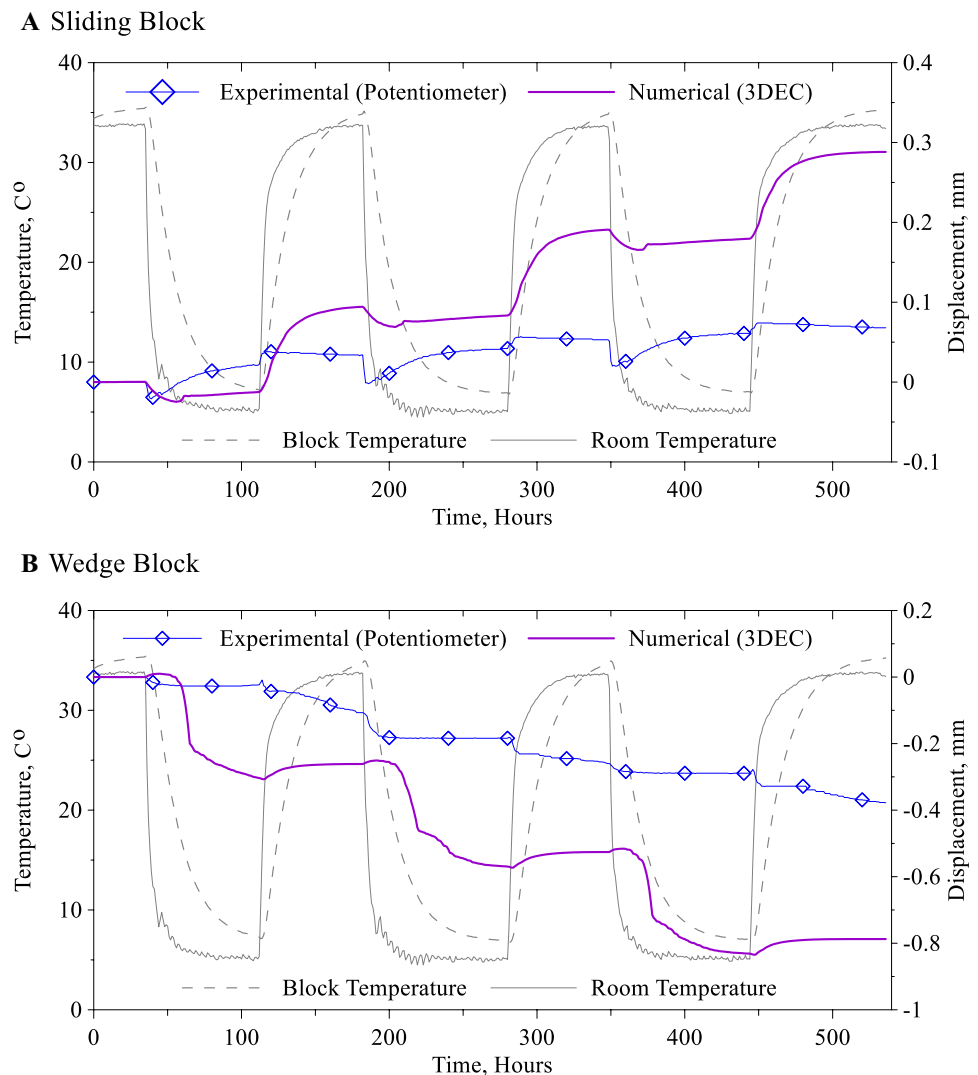
were mounted, and compared with the actual displacement obtained in the experiments.

Local damping is used in our simulations. In this scheme, the damping force is proportional to the magnitude of the unbalanced force. This method is preferred in cases involving sudden load changes, thermal loads in our case, or progressive failure (Itasca Consulting Group 2013). Due to the rapid changes of boundary temperature, the number of mechanical steps for each thermal step is increased to ensure that the model remains in a quasi-static mechanical equilibrium mode.

3.1 Numerical Validation

To examine the response of the system to temperature fluctuations the measured temperature in the climatically controlled room was applied to the outer boundaries of the numerical model to represent three cycles of heating and cooling, or three whole years (three cycles of summer and

Fig. 8 Comparison between numerical 3DEC results (purple lines) and physical model results (blue lines). Displacement (colored lines) is shown on the right y-axis, room and block temperature (gray lines), as recorded inside the CCR are shown on the left y-axis, for **a** Sliding Block, and **b** Wedge Block (color figure online)



winter). The numerical displacements of the sliding block and the wedge are compared in Fig. 8 to the displacements obtained for the physical model as recorded by the potentiometer displacement transducers in measurement areas 1 and 2 (see locations in Fig. 5a). The numerical analyses show that when temperature is increased, the toe of the block moves down the inclined plane (Fig. 8a). When temperature drops, the sliding block contracts, allowing the wedge to slide further into the opening aperture (Fig. 8b). The wedge is not sliding up the joint and the block motion continues in the same direction for the consequent cycles.

In this particular simulation, which was performed with the thermo-mechanical parameters exactly as measured in the laboratory, the sliding block displacement at the toe as computed by 3DEC is greater than the displacements obtained experimentally for the physical model at measurement area 1. Yet, the numerical model captures the expected physics of the failure mode very well, and the numerical displacements are well within the same order of magnitude as obtained experimentally. To better understand the relative influence of the controlling parameters we perform sensitivity analyses in the next section.

3.2 Sensitivity Analyses

The discrepancy between numerical and physical model displacements may be attributed in part to input thermo-mechanical properties derived from laboratory tests we conducted. To examine the sensitivity of the simulation to changes in key thermo-mechanical parameters, sensitivity analyses are conducted. In these simulations, the same model is subjected to the same boundary temperature. In each simulation the value of the analyzed parameter is changed, while the rest of the parameters are kept constant at the reference values (Table 1). The cumulative displacement at the end of each simulation is used to examine the sensitivity of the numerical model to the different properties.

Thermocouple measurements in the laboratory show that each heating or cooling cycle is long enough for the entire model to reach uniform temperature. The same holds in the numerical simulation of the laboratory experiment that uses the estimated thermal conductivity value. As long as a uniform temperature is reached at the end of a heating or cooling cycle, a change in thermal conductivity is not expected to have a significant effect for the size of the block analyzed at the lab, and the sensitivity of the model to this parameter is therefore not examined. The sensitivity of the numerical model results to changes in shear and normal joint stiffness, joint friction angle, elastic modulus of the block, and the thermal expansion coefficient is illustrated in Fig. 9.

As would be intuitively expected, with increasing joint shear stiffness (Fig. 9a) and friction angle (Fig. 9b) the accumulated block displacement at the toe decreases.

Interestingly, however, increasing normal stiffness results in greater displacement at the lower range tested, but for values typical to rock-to-rock interfaces (greater than 1 MPa/mm), the displacement remains relatively constant.

Similar to the effect of joint shear stiffness, the accumulated toe displacement clearly decreases with increasing block material stiffness (Fig. 9c), suggesting that more thermal strain is absorbed with increasing Young's modulus.

The block displacement computed with 3DEC appears to be the most sensitive however to the thermal expansion coefficient value (Fig. 9d). While the displacement would be expected to increase with increasing thermal expansion coefficient, in fact it peaks at a value close to the value measured in the lab and then it decreases with increasing thermal expansion coefficient. We believe the thermal expansion coefficient value at which the displacement peaks greatly depends on the geometrical configuration and on the thermo-mechanical properties used in the simulation. With high values of thermal expansion coefficient, the blocks in the system contract significantly during cooling periods, including the rock mass and the wedge. This enables block motion up the sliding plane to be measured at the toe. Such "up slope" contraction is restrained with lower thermal expansion coefficient, mainly due to frictional resistance and shear stiffness.

The sensitivity analyses reveal that the computed displacements with 3DEC are most sensitive to the thermal expansion coefficient. The discrepancy between the measured and computed displacements could be due to the resolution and accuracy of the laboratory measurement of the thermal expansion coefficient, and, to some degree, due to the change in the other thermo-mechanical properties. In contrast to the analytical solution, the numerical model takes into account the thermal expansion coefficient in 3D and more closely simulates the physical phenomenon. Another source for the discrepancy may be related to numerical inaccuracy, mainly due to the rapid changes of boundary temperature in the physical model experiments that are not captured properly in the numerical model.

3.3 The influence of the Wedge in the Tension Crack

We believe that part of the accumulated displacement of the sliding block down the sliding interface is due to the so called "crawling motion" suggested by Gunzburger et al. (2005) and briefly described in the introduction. Based on the experimental and numerical results we achieved thus far, it would be instructive to compare the relative significance of the two thermally induced failure mechanisms, "crawling" vs. "wedging–ratcheting", on the cumulative displacement of blocks prone to these two failure modes.

We use the same physical model to analyze the two failure modes. Two block configurations are simulated, one with a wedge in the tension crack and another without the

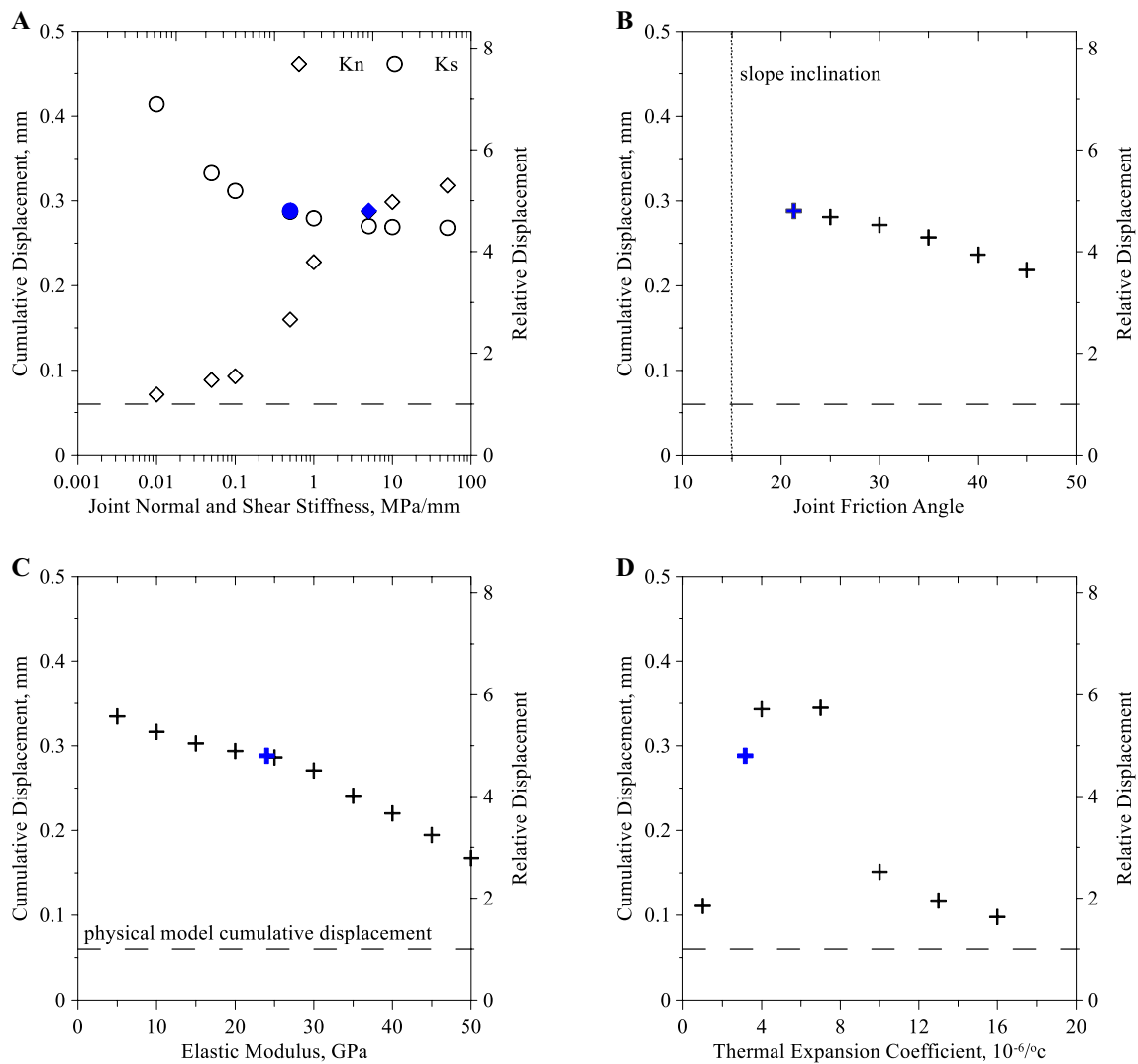


Fig. 9 Sensitivity analyses of 3DEC results to key thermo-mechanical properties. Dashed horizontal lines denote the accumulated displacement of the sliding block as obtained experimentally. **a** normal and shear stiffness of the joints, **b** friction angle of joints; dotted vertical

line denotes the inclination of the sliding plane, **c** elastic modulus of block material, **d** thermal expansion coefficient of block material. Blue (bold) symbols denote the value of the key parameter values determined experimentally by us (color figure online)

wedge, the latter in order to represent a simple problem of a block on an inclined plane subjected to temperature oscillations. The same temperature log is applied to the boundaries in both configurations. The input temperature history and the displacement of the sliding block toe in the two geometrical configurations as modeled with 3DEC are shown in Fig. 10. The 3DEC results reveal that the displacement due to the wedging–ratcheting mechanism is three times greater than the “crawling motion” for the test conditions considered in the analysis including block size, thermo-mechanical properties, and applied temperature cycles. A similar ratio between the displacements of both

mechanisms was also observed in the physical model without the wedge in the tension crack. A comparison between the cumulative displacements of the sliding block at the end of each thermal cycle as obtained with the numerical and physical models is shown in Fig. 11. The difference between the two mechanisms is significant for the cases investigated here. It is explained by the mere presence of the wedge in the joint: the wedge offers a back support that forces directional sliding of the block towards the free surface during the heating phase. We conclude, therefore, that the wedging–ratcheting mechanism has a significant contribution to the overall displacement of the sliding block.

Fig. 10 Comparison between two different thermally induced failure mechanisms as computed with 3DEC, the “crawling motion” (Gunzburger et al. 2005) without a wedge in the tension crack and the “wedging–ratcheting” mechanism” with a wedge in the tension crack. Solid line denotes the temperature applied to the model boundaries in both simulations

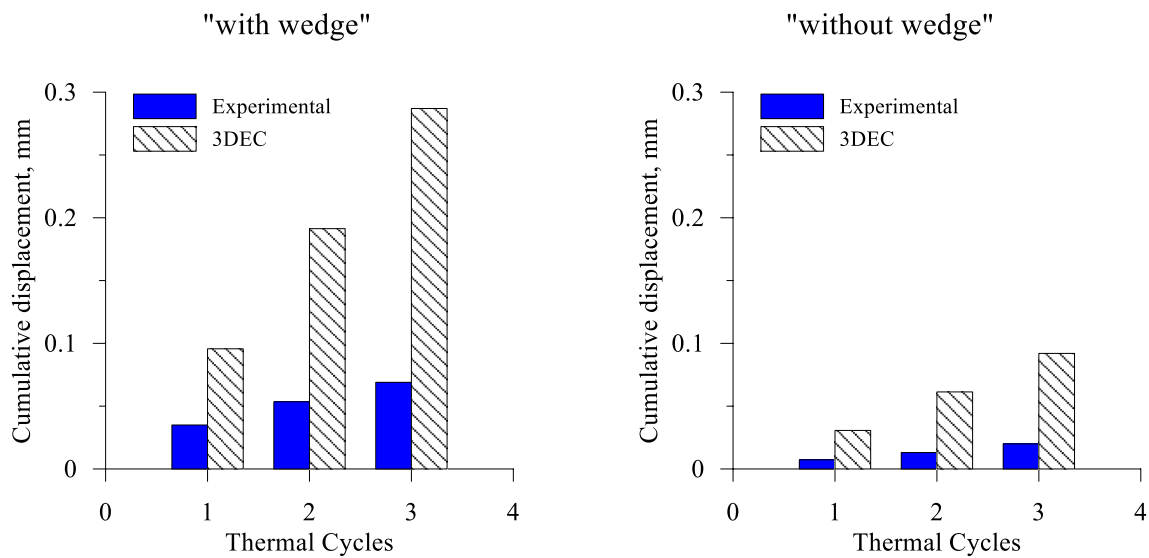
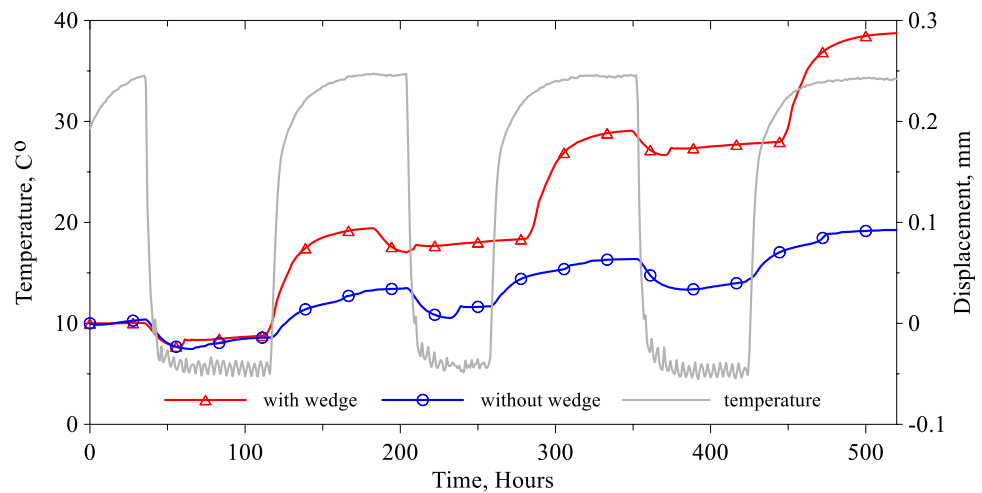


Fig. 11 Cumulative displacements for each thermal cycle as obtained with the numerical and physical models for the “wedging–ratcheting” (left) and Crawling (right) failure mechanisms

4 Field Case Study

4.1 Geological Setting

The Masada world heritage site is located on the west margins of the Dead Sea rift valley. The monument attracts nearly one million tourists each year. In 1998, during the construction of a new cable car station at the East face of the mountain (immediately above the old station at the top of the locally known “Snake Path cliff”—see Fig. 12a), an abrupt displacement of a large block was detected from the output of installed joint meters at the site. This event

prompted reinforcement of the block along with the entire segment of the Snake Path cliff.

Mount Masada, an uplifted horst, is situated in a seismically active region and consequently has experienced many earthquakes in its history. One could assume, therefore, that the detected displacements of the block in 1998 were of seismic origin. We analyze in this section the previously recorded episodic motion of this block in terms of the newly studied wedging–ratcheting mechanism to see if this failure mode alone could be responsible to the detected displacement episode, before the block was anchored to the rock mass.

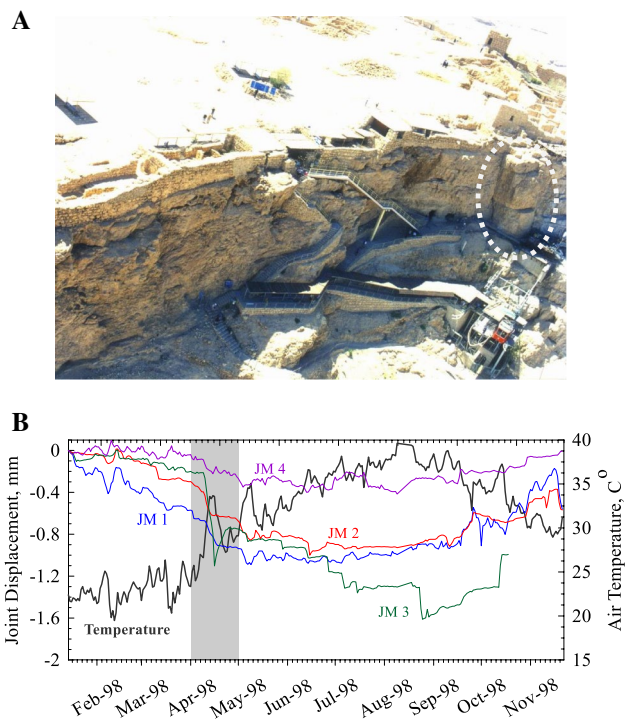


Fig. 12 **a** View of the snake path cliff in Masada and the old cable car station as of 1998. The studied block is delineated in dashed line. **b** Monitored block displacement (colors) and temperature (black) in 1998 (Hatzor 2003). The abrupt displacement episode (see text) is shaded (color figure online)

Masada Mountain consists of strong limestones and dolomites of the upper cretaceous Judea Group of central Israel. The rock mass, however, is highly discontinuous and consists of several persistent joint sets, the intersections of which create removable blocks that pose a risk to the bridge that connects between the new cable car station and the entrance to the site at the top of the snake path cliff (Fig. 13a). The block that rests directly above the new bridge (delineated in Figs. 12a, 13a) was identified as hazardous during site investigations for the new cable car complex in the late 1990's and an extensive research campaign was thus conducted to investigate potential failure modes, current factor of safety, and alternative support measures. The block, referred to as "Block 1" by Hatzor (2003), was permanently anchored to the rock mass in 1999.

The East face of Mount Masada is intersected by two orthogonal sets of sub vertical and persistent joints, one striking NNE (J2) and the other striking ESE (J3). The spacing between joints in each set are between 5 and 10 m. The bedding planes set (J1) dips 20° to SE. The study of the East face of Mount Masada by Hatzor (2003) was complemented by Bakun-Mazor et al. (2013) for the West face of Masada. These two studies provide, in addition to joint displacement

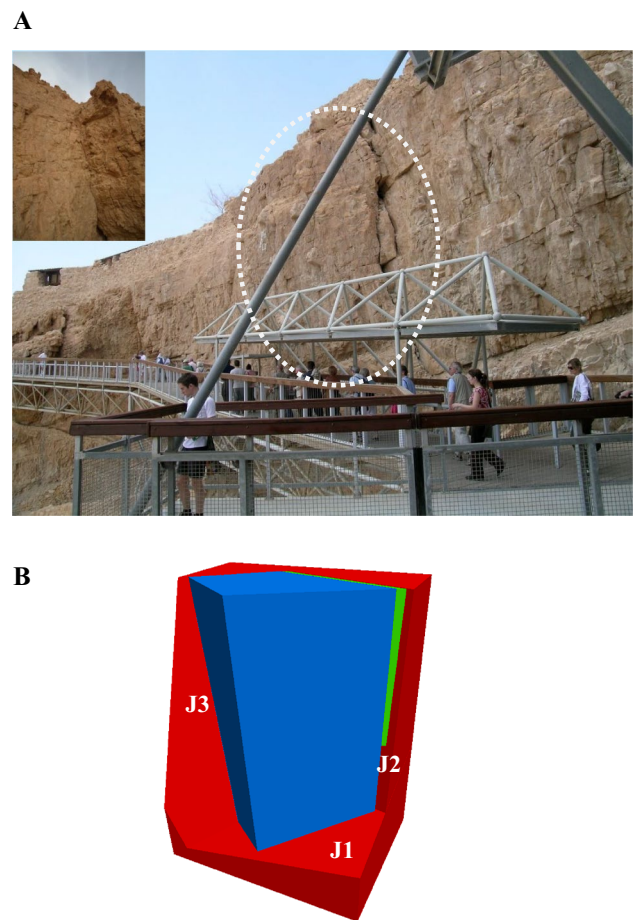


Fig. 13 **a** The analyzed block (dashed) and the bridge at the top of the snake path cliff today. J2 with the wedge block is visible in the view direction. The trace of J3 with no wedge blocks is shown in inset. **b** 3DEC model of the block used in this study

monitoring data, also mechanical and physical parameters of the intact rock material and the discontinuities (Table 2).

The geometry of Block 1 as analyzed here is adopted from Hatzor (2003). The studied block is relatively large, with height of 15 m and depth of 6 m in the direction of sliding. It rests on a moderately dipping bedding plane and is separated from the rock mass by members of J2 and J3 which for simplicity we shall refer to them here as J2 and J3. J2 is filled with rock fragments of various sizes in its upper part, and with softer rock and soil at the bottom (Fig. 13a). Across J2 a total displacement of 20 to 40 cm has accumulated over its geological history. J3 is tight and from field mapping it appears that sliding across it that accompanied the opening of J2 commenced with no opening or dilation across it (see inset in Fig. 13a).

Four LVTD type joint meters were installed in 1998 across the sub-vertical joints, three across J2 (JM1, JM2, and JM3) and one across J3 (JM4) to measure relative

Table 2 Properties of the removable block in Masada

| | Parameter | Symbol | Units | Value | Sources |
|---------------------|-------------------------------|---------------|--------------------|--------|---------------------------|
| Block geometry | Bedding plane | J_1 | dip/dip direction | 20/124 | Hatzor (2003) |
| | Joint 2 | J_2 | – | 84/107 | |
| | Joint 3 | J_3 | – | 75/052 | |
| | Face surface 1 | f_1 | – | 84/060 | |
| | Face surface 2 | f_2 | – | 90/126 | |
| | Block volume | V | m^3 | 563 | |
| Material properties | Elastic modulus | E | GPa | 40 | Bakun-Mazor et al. (2013) |
| | Poisson's ratio | ν | – | 0.2 | |
| | Bulk density | ρ | kg/m^3 | 2600 | |
| | Block mass | W | 10^6 kg | 1.465 | |
| Joints properties | Peak friction angle | ϕ_{peak} | $^\circ$ | 41 | Hatzor (2003) |
| | Saw-cut friction angle | ϕ_{saw} | $^\circ$ | 28 | |
| | Residual friction angle | ϕ_{res} | $^\circ$ | 23 | |
| | Normal stiffness | K_n | GPa/m | 5 | Bakun-Mazor et al. (2013) |
| | Shear stiffness | K_s | GPa/m | 1 | |
| Thermal properties | Thermal expansion coefficient | α | $10^{-6}/^\circ C$ | 6–8 | Bakun-Mazor et al. (2013) |
| | Thermal conductivity | λ | W/m/K | 1.7 | |
| | Thermal diffusivity | D_T | $10^{-7}m^2/sec$ | 8.07 | Calculated |
| | Specific heat capacity | C_p | J/kg/K | 810 | Rohsenow et al. (1998) |

displacement between the rock mass and Block 1. Relative humidity and platinum thermo-resistance meters were also placed in the aperture of J2 in 1998 to monitor relative humidity and temperature. The abrupt displacement event mentioned above occurred in April 1998 when a sudden increase in temperature was recorded in the region, and it was captured by the monitoring system installed on Block 1. The total displacement of Block 1 during this sudden thermal event amounted to ~ 1 mm (see Fig. 12b). Note that at December 1998 Block 1 was permanently anchored to the rock mass and therefore a complete thermal cycle and displacement response could not be obtained, as the installed monitoring system ceased to operate once the anchoring of the block was complete. To enable a complete analysis of the response of Block 1 to temperature changes with 3DEC we use, therefore, a complete temperature log from the Israel Meteorological Service (2017) recorded in the region between the years 2012 and 2015.

4.2 3DEC Model of Block 1

The geometry of Block 1 and its surrounding are reproduced in 3DEC using the data from Table 2. Two friction angle values are used to represent the frictional resistance of the joints, peak and residual, as obtained from direct shear tests of rough bedding plane interfaces and from triaxial tests of filled saw-cut planes, respectively (Hatzor 2003; Hatzor

et al. 2004). Although initial sliding commenced with the original roughness profile preserved, since the block has displaced more than 200 mm in its geological history we also consider the displacement of the block under residual friction conditions.

The wedge block in J2 is modeled here as a single prismatic wedge occupying the full width of the crack from its top down to the lower third of the joint height (Fig. 13b). The rock mass is fixed (no velocity in all directions) for the entire simulation, whereas Block 1 and the wedge block are free to move. The initial temperature of the blocks is assumed uniform and is set to $27^\circ C$.

Blocks are discretized using a uniform mesh with an average tetrahedron edge length of 30 cm, about 5% of the sliding block length in the direction of sliding. After initial equilibrium is reached in the model, the temperature history obtained between 2012 and 2015 by the Israel Meteorological Service (2017) Ein-Gedi station, located 15 km from the site, is applied to the outer boundaries of the blocks to simulate the response of the system to a full cycle of heating and cooling. The displacement of the center of mass of Block 1 parallel to the dip direction of J1 is recorded during the 3DEC simulations and the results obtained for peak and residual friction are shown in Fig. 14.

We find that the displacement of the block center occurs mainly during the heating phases. During these periods the block expands, compressive stresses develop around the

Fig. 14 Thermally induced displacements of the center of mass of the analyzed block (Block 1) in direction parallel to the dip of the sliding (bedding) plane as computed with 3DEC for peak and residual (saw-cut) friction. The applied temperature to the block boundaries is shown on the upper panel; the compressive normal stresses that evolve at the back of the wedge in response to thermal oscillations, are shown on the lower panel

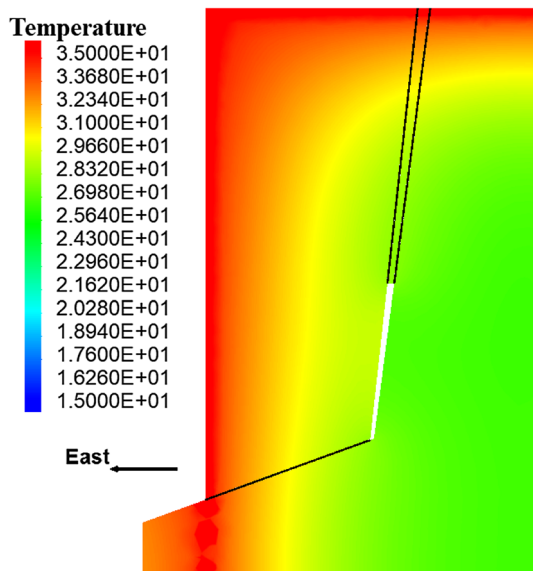
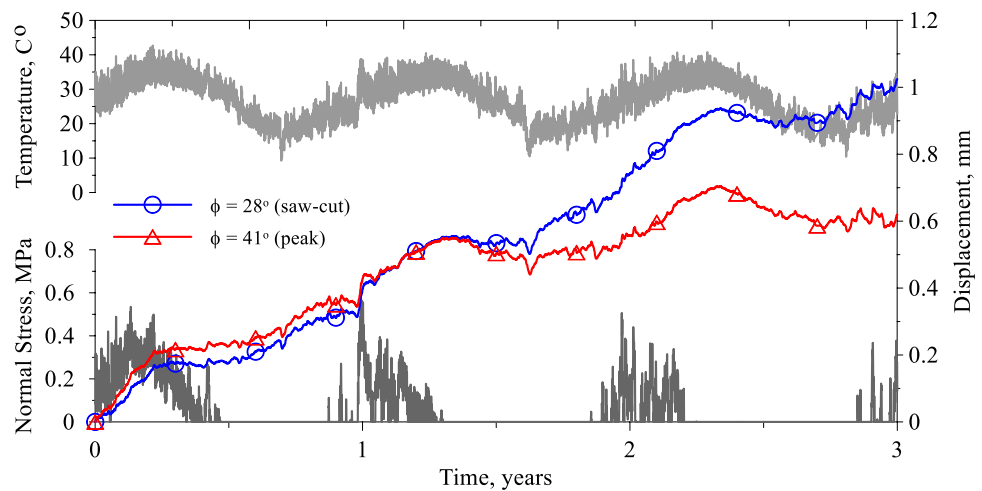


Fig. 15 Cross section through Block 1 showing temperature contours when annual temperature peaks. Thermal conductivity is not high enough for the block to reach uniform temperature

wedge (see lower panel of Fig. 14), and the locked position of the wedge in the joint prompts further displacement of the block down the sliding surface. The cumulative displacement over the three years analyzed is 0.6 or 1 mm for assumed peak or residual friction across the inclined sliding plane, respectively.

Finally, we find that given the input thermo-mechanical parameters assumed in our 3DEC simulations, the temperature distribution within the block does not reach a uniform value during the thermal cycles (see Fig. 15). We could expect, therefore, greater annual displacements in rocks with greater thermal conductivity.

5 Discussion

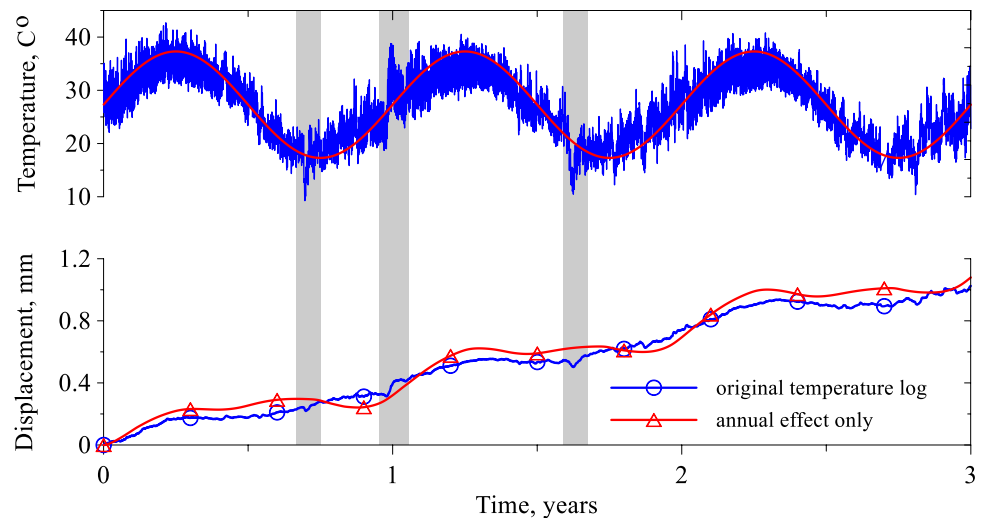
5.1 Annual Block Displacement

The annual displacement of Block 1 in Masada, as obtained by field measurements and 3DEC simulations, is rather small (about 1/3 mm per year), and for sustainability of engineering structures with a design life time of 50 years may be considered negligible. For natural rock slopes, however, this rate may lead to significant displacements over geological time scales, and advance the deterioration rate of the rock mass. We therefore wish to understand the cumulative nature of the wedging–ratcheting mechanism over long periods of time.

The removable block slides down the slope, according to the numerical analysis presented in the previous section, at a rate of 0.21–0.34 mm per year, depending on the assumed frictional resistance across the sliding surface. The most important feature presented in Fig. 14, however, is the irreversible nature of this displacement. In each phase of displacement, the wedge slides further down the opening joint, preventing block displacement back up the slope; once the wedge takes its place in the joint, it does not move up, only down. The small magnitude of annual displacement and its slow rate is of little significance in the short term (tens of years). However, since the displacement is irreversible, it can accumulate and become significant over centuries, assuming the opening joint is continuously filled with new rock fragments over time.

It is interesting to determine whether daily temperature fluctuations play a significant role in the total accumulated displacement. For this purpose, the daily temperature input record used in the simulation described earlier is now represented by a fitted sinusoidal function (red line in the upper panel of Fig. 16) to smooth the temperature signal, and the

Fig. 16 The influence of short term thermal fluctuations on block displacement. Up) Temperature input for the simulations. Bottom) Computed block displacement with 3DEC for the two input temperature records



system response is reanalyzed for the residual friction value of 28 degree. We find that displacements obtained with and without temperature smoothing are essentially the same, the difference amounting to less than 5% in cumulative displacement after 3 years. It could perhaps be concluded that for the cases analyzed here, daily temperature fluctuations do not play a significant role in the overall mechanism because the heat does not propagate deep enough into the rock in short, day long, exposure periods to cause significant expansion or contraction. It should be kept in mind, however, that high frequency changes such as daily temperature fluctuations can become more significant in smaller blocks or rocks with greater thermal conductivity, as a larger portion of the block will be influenced by the temperature changes.

As predicted by the wedging–ratcheting mechanism, most of the displacement occurs when the temperature is rising, during the transition from winter to summer. However, some displacement can also be observed during winter, due to short periods of intra-seasonal heating episodes, see for example the third shaded area from the left in Fig. 16. This can be associated with the displacement mode introduced by Taboada et al. (2017) described in the introduction, in which short-term thermal cycles of between 2 and 15 days can cause thermally induced displacements. Such instances are shown as shaded areas in Fig. 16. An effect of this type can explain the relatively large displacement of ~1 mm measured for Block 1 by Hatzor (2003) in April–May 1998 (see shaded area in Fig. 12b). It should be pointed out that the incremental displacement measured by Hatzor (2003) is larger than the displacement predicted by 3DEC for intra-seasonal temperature change. The discrepancy could be due to the fact that the exact orientation of the joint meters and therefore the orientation of the actual displacement vector measured in the field is not known today. Therefore a comparison between individual joint meter outputs from the field monitoring campaign and the computed displacement of the

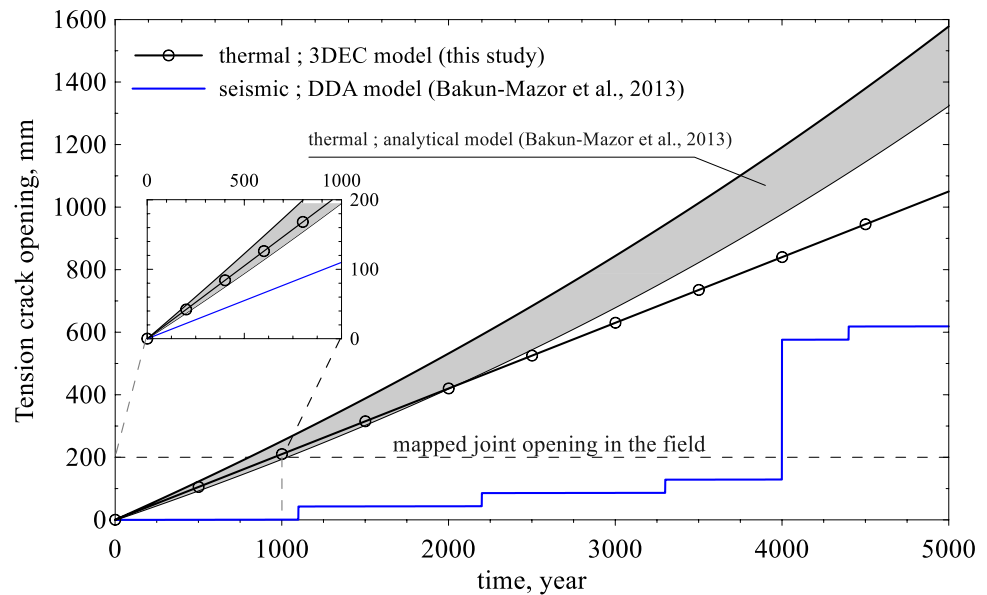
centroid of Block 1 with 3DEC can only be qualitative, at best.

5.2 Thermal vs. Seismically Induced Block Motion

The location of Mount Masada near the active Dead Sea fault calls for consideration of seismically induced displacements and comparison to the thermally induced mechanisms. Bakun-Mazor et al. (2013) studied the response of Block 1 to dynamic loading using the numerical, discrete elements Discontinuous Deformation Analysis (DDA) method (Shi 1993). Using an input motion based on the 1995 Nuweiba earthquake (for details see Hatzor et al. 2004), they determined numerically the expected displacement of Block 1 that would have been caused by earthquake of magnitude of 6 to 7.5 in the Dead Sea valley at a distance of 1 km from Mount Masada. They found the expected accumulated displacement of Block 1 during a single event based on the input motion that includes the topographic effect of Masada that was measured in the field by Hatzor et al. (2004). The recurrence time of moderate ($M_w = 6.5$) and strong ($M_w = 7$) earthquakes was assumed to be 1100 and 4000 years, respectively, based on the local seismicity of the region (Begin 2005; Shapira et al. 2007). The expected total accumulated displacement in a 5000 year window can therefore be compared for both seismic and thermally induced mechanisms.

The displacement of Block 1 over a period of 5000 years in response to climatically controlled wedging–ratcheting mechanism as computed with 3DEC in this study, and to seismically induced ground motions at the top of Masada as computed with DDA by Bakun-Mazor et al. (2013) is shown in Fig. 17. The thermally-induced wedging–ratcheting displacement, as calculated by Bakun-Mazor et al. (2013) using the analytical model, is also presented for reference. For the wedging–ratcheting mechanism obtained numerically using 3DEC, a uniform annual rate of displacement of 0.21 mm/

Fig. 17 The displacement of Block 1 over a period of 5000 years in response to climatically controlled wedging–ratcheting mechanism and to seismically induced ground motions (after Bakun-Mazor et al. 2013)



year is assumed with the sinusoidal input temperature over the time span analyzed. It is important to point out that the slip rate can change over such a long period in both mechanisms, as the wedge volume may increase and the frictional resistance of the sliding surface may deteriorate over time. Moreover, the temperature history of the analyzed time span of 5000 years may not follow the harmonic sinusoidal pattern assumed here.

We find that the total cumulative displacement of Block 1 over a time span of 5000 years due to the wedging–ratcheting mechanism is greater than the seismically induced displacement, when everything else is equal. The cumulative nature of the wedging–ratcheting mechanism makes the thermally induced displacement significant in terms of long-term geomorphology, even when compared with seismic triggering, in an area considered seismically active, such as the Dead-Sea Transform. Therefore, it is found that the wedging–ratcheting mechanism has an important role in shaping the landscape, and is indeed a failure mode that cannot be ignored when considering long term rock slope instability.

6 Summary and Conclusions

We examine the thermally induced wedging–ratcheting mechanism using physical model inside a Climate Controlled Room, and the numerical distinct element method in three dimensions (3DEC). First, we validate the numerical results with laboratory experiments, and then, we analyze a case study from Mount Masada, Israel. We obtained the following significant results:

1. The thermally induced wedging–ratcheting mechanism is proven to cause irreversible displacement down an inclined slope. Heating phases are linked with expansion of the blocks in the system, resulting in compressive stress development against the wedge, enhancing block displacement down the sliding interface. Cooling phases are associated with block contraction, resulting in joint opening and further sliding of the wedge down the aperture of the tension crack behind the sliding block.
2. The numerical 3DEC platform used in this research is proven valid for the purposes of this study. The sensitivity of the results to the choice of thermo-mechanical parameters, particularly the thermal expansion coefficient has been explored.
3. The results obtained from the analytical model (Pasten 2013) are compared to the experiment results and numerical simulations, in terms of permanent block displacement at the end of each thermal cycle. It is shown that the results from the analytical model match the numerical simulations, and both predict a cumulative displacement rate 4 times greater than measured in the lab. The theoretical results obtained are nevertheless in the same order as the results measured in the lab, and the discrepancy is attributed to the greater sensitivity of the theoretical solutions to the exact values of the input parameters, primarily the linear thermal expansion coefficient.
4. The complexity of the geometrical configurations of the block system under investigation makes an analytical solution for this problem very challenging. However, a comprehensive study of the configuration

and geometry of a problem in the field, accompanied by laboratory tests and experiments to determine the thermo-mechanical properties of the rock, can lead to an educated numerical simulation that produces a reliable result.

5. The proposed wedging–ratcheting mechanism brings an additional contribution to the total displacement of the block, compared with other known thermally (e.g. crawling motion) or seismic induced mechanisms.
6. The proposed failure mechanism can play a significant role in shaping natural rock slopes over time due to the cumulative and repetitive nature of the incremental displacements over geological time periods.

Acknowledgements This research is funded by Israel Science Foundation through contract no. ISF—1442/13. Prof. Noam Weisbrod from Zuckerberg Institute for Water Research, Blaustein Institutes for Desert Research at Ben-Gurion University of the Negev, is thanked for allowing us to use the Climatic Controlled Room in his lab and for assistance with the setup of the physical model.

Compliance with Ethical Standards

Conflict of interest The authors declare that they have no conflict of interest.

Appendix 1

We derive here the maximum sliding force required to reach limit equilibrium along the sliding surface (F_{max}). Consider the free body diagrams for the sliding and wedge blocks as shown in Fig. 18 in Appendix 1.

The driving forces acting on the sliding and the wedge blocks are:

$$W_1 \sin \eta_1 + W_2 \sin \eta_1 + F_{max} \tag{6}$$

The resisting friction forces parallel to the sliding plane are f_1 and f_2 . In order to find f_2 , consider the force polygon in Fig. 18 in Appendix 1 showing the weight of the wedge W_2 and the reactions along the wedge faces R and T :

$$\frac{W_2}{\sin(90 - \eta_2)} = \frac{T}{\sin(90 - \eta_1)} \Rightarrow T = W_2 \frac{\cos \eta_1}{\cos \eta_2} \tag{7}$$

The friction force due to the reaction T , is:

$$f_T = T \tan \phi = W_2 \frac{\cos \eta_1}{\cos \eta_2} \tan \phi \tag{8}$$

The component of f_T parallel to the sliding plain, is:

$$f_2 = f_T \cos \eta_2 = W_2 \cos \eta_1 \tan \phi \tag{9}$$

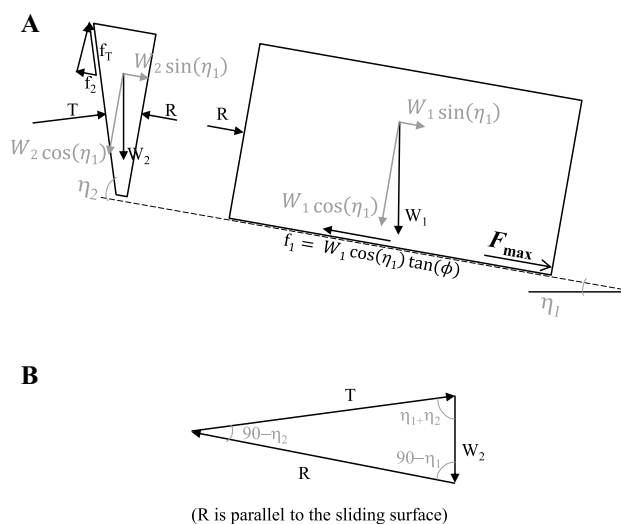


Fig. 18 a Free body diagrams of the sliding and the wedge blocks, b force polygon on the wedge block

Therefore, the total resisting frictional forces parallel to the sliding plane are:

$$f_1 + f_2 = W_1 \cos \eta_1 \tan \phi + W_2 \cos \eta_1 \tan \phi \tag{10}$$

From limit equilibrium parallel to the sliding plane, we obtain the magnitude of F_{max} :

$$F_{max} = W_1 \cos \eta_1 \tan \phi + W_2 \cos \eta_1 \tan \phi - W_1 \sin \eta_1 - W_2 \sin \eta_1 \tag{11}$$

Inserting the blocks weights:

$$W_1 = L_b H_b \gamma; W_2 = \frac{L_{w1} + L_{w2}}{2} H_w \gamma$$

We get:

$$F_{max} = (L_b H_b \gamma) (\cos \eta_1 \tan \phi - \sin \eta_1) + \frac{L_{w1} + L_{w2}}{2} H_w \gamma [\cos \eta_1 \tan \phi - \sin \eta_1] \tag{12}$$

$$F_{max} = \gamma (\cos \eta_1 \tan \phi - \sin \eta_1) \left[L_b H_b + \frac{L_{w1} + L_{w2}}{2} H_w \right]$$

References

Bakun-Mazor D, Hatzor YH, Glaser SD, Carlos Santamarina J (2013) Thermally vs. seismically induced block displacements in Masada rock slopes. *Int J Rock Mech Min Sci* 61:196–211
 Begin ZEB (2005) Destructive earthquakes in the Jordan Valley and the Dead Sea: their recurrence intervals and the probability of their occurrence. Geological Survey of Israel, Jerusalem
 Cundall PA (1988) Formulation of a three-dimensional distinct element model—Part I. A scheme to detect and represent contacts in a

- system composed of many polyhedral blocks. *Int J Rock Mech Min Sci Geomech Abstr* 25:107–116
- Cundall PA, Hart RD (1992) Numerical modelling of discontinua. *Engineering computations* 9(2):101–113
- ENCARDIO RITE. (2015). products. <https://www.encardio.com/products/geotechnical/displacement/crack-meter-displacement.php>
- Feldheim A (2017) Experimental study of thermally induced wedging–ratcheting mechanism in rock slopes. Master Thesis, Geological and Environmental Sciences, Ben-Gurion University of the Negev, Beer Sheva. P 58
- Gischig VS, Moore JR, Evans KF, Amann F, Loew S (2011a) Thermo-mechanical forcing of deep rock slope deformation: 1. Conceptual study of a simplified slope. *J Geophys Res Earth Surf* 116:F04010
- Gischig VS, Moore JR, Evans KF, Amann F, Loew S (2011b) Thermo-mechanical forcing of deep rock slope deformation: 2. The Randa rock slope instability. *J Geophys Res Earth Surf* 116:F04011
- Greif V, Sassa K, Fukuoka H (2006) Failure mechanism in an extremely slow rock slide at Bitchu-Matsuyama castle site (Japan). *Landslides* 3(1):22–38
- Greif V, Simkova I, Vlcko J (2014) Physical Model of the Mechanism for Thermal Wedging Failure in Rocks. In: Sassa K, Canuti P, Yin Y (eds) *Landslide science for a safer geoenvironment*. Springer, New York, pp 45–50
- Gunzburger Y, Merrien-Soukatchoff V, Guglielmi Y (2005) Influence of daily surface temperature fluctuations on rock slope stability: case study of the Rochers de Valabres slope (France). *Int J Rock Mech Min Sci* 42(3):331–349
- Hart R, Cundall P, Lemos J (1988) Formulation of a three-dimensional distinct element model—Part II. Mechanical calculations for motion and interaction of a system composed of many polyhedral blocks. *Int J Rock Mech Min Sci Geomech Abstr* 2:117–125
- Hatzor YH (2003) Keyblock stability in seismically active rock slopes - Snake Path cliff, Masada. *J Geotech Geoenviron Eng* 129(8):697–710
- Hatzor YH, Arzi AA, Zaslavsky Y, Shapira A (2004) Dynamic stability analysis of jointed rock slopes using the DDA method: King Herod's Palace, Masada, Israel. *Int J Rock Mech Min Sci* 41(5):813–832
- Hatzor YH, Talesnick M, Tsesarsky M (2002) Continuous and discontinuous stability analysis of the bell-shaped caverns at Bet Guvrin, Israel. *Int J Rock Mech Min Sci* 39(7):867–886
- Israel Meteorological Service. (2017). Israel Meteorological Service Data Base.
- Itasca Consulting Group I (2013) 3DEC—three-dimensional distinct element code (Version 5.0), user's guide. Itasca, Minneapolis
- Jing L (2003) A review of techniques, advances and outstanding issues in numerical modelling for rock mechanics and rock engineering. *Int J Rock Mech Min Sci* 40(3):283–353
- Mufundirwa A, Fujii Y, Kodama N, Kodama J (2011) Analysis of natural rock slope deformations under temperature variation: a case from a cool temperate region in Japan. *Cold Reg Sci Technol* 65(3):488–500
- Pasten C (2013) Geomaterials subjected to repetitive loading: implications on energy systems. PhD thesis, Georgia Institute of Technology, Atlanta. P 149
- Pasten C, García M, Cortes D (2015a) Physical and numerical modelling of the thermally induced wedging mechanism. *Geotech Lett* 5(3):186–190
- Pasten C, García M, Santamarina C (2015b) Thermo-mechanical ratcheting in jointed rock masses. *Géotechn Lett* 5:86–90
- Rohsenow WM, Hartnett JP, Cho YI (1998) *Handbook of heat transfer* 3. McGraw-Hill, New York
- Shapira A, Hofstetter R, Abdallah A-QF, Dabbeek J, Hays W (2007) Earthquake hazard assessments for building codes. *Institutions* 3:8
- Shi G-H (1993) Block system modeling by discontinuous deformation analysis 1.1. *Computational Mechanics*, Boston
- SIM STRUMENTI. (2009). Products. <https://www.simstrumenti.com/en/products.html>.
- Taboada A, Ginouvez H, Renouf M, Azemard P (2017) Landsliding generated by thermomechanical interactions between rock columns and wedging blocks: study case from the Larzac Plateau (Southern France). In *EPJ Web of Conferences*, (14012). EDP Sciences.
- Vargas JE, Velloso R, Chávez L, Gusmão L, Amaral C (2013) On the effect of thermally induced stresses in failures of some rock slopes in Rio de Janeiro. *Braz Rock Mech Rock Eng* 46(1):123–134
- Vicko J, Greif V, Grof V, Jezny M, Petro L, Brcek M (2009) Rock displacement and thermal expansion study at historic heritage sites in Slovakia. *Environ Geol* 58(8):1727–1740
- Watson A, Moore D, Stewart T (2004) Temperature influence on rock slope movements at Checkerboard Creek. In: *Proceedings of the 9th International Symposium on Landslides*, (6). London: Taylor & Francis Group, Rio de Janeiro

Publisher's Note Springer Nature remains neutral with regard to jurisdictional claims in published maps and institutional affiliations.